

An Analytical Range-Angle Dependent Beam Focusing Model for Terahertz Linear Antenna Array

Lingxiang Li, Haoran Li, Zhi Chen, *Senior Member, IEEE*,
Weixin Chen, Shaoqian Li, *Fellow, IEEE*

Abstract

This paper considers a scenario in which the Terahertz (THz) transmitter equipped with a linear antenna array wishes to focus its beam to a desired spatial region in the array near-field. The goal is to compute the achievable spatial region and determine how the system parameters such as the carrier frequency, the array dimension and the user's location affect its beam focusing performance. First, based on a theorem from analytic geometry, we show that the achievable focusing spatial region constitutes a rotated ellipse, with the x and y coordinates denoting the range and angle, respectively. In this way, the determination of the spatial region is reduced to a problem of deriving the coverage of an ellipse. The achievable coverage is then obtained in closed form, and the construction of carrier frequency offsets that can analytically control the beam focusing performance is provided. Numerical results validate the theoretical findings and demonstrate the performance of the proposed method.

Index Terms

THz communication, Large-scale antenna arrays, Beam focusing, Near-field, The sixth generation (6G).

I. INTRODUCTION

The sixth generation (6G) wireless systems are expected to support emerging new applications such as augmented reality (AR), virtual reality (VR), and connected autonomous systems [1]. These bandwidth-intensive applications require the delivery hundreds of gigabits per second, and

Lingxiang Li, Haoran Li, Zhi Chen, Weixin Chen and Shaoqian Li are with the National Key Laboratory of Science and Technology on Communications, UESTC, Chengdu 611731, China (e-mails: {lingxiang.li, chen_zhi}@uestc.edu.cn).

This work was supported in part by the National Natural Science Foundation of China under Grant U21B2014.

sensing resolution at the millimeter level. Terahertz (THz) band can provide hundreds of GHz bandwidth and thus is promising in meeting those requirements [2], [3]. However, to enjoy the advantage of broad bandwidth of THz in 6G, some difficulties still need to be resolved, since THz signals suffer from: (i) inherently severe propagation loss; (ii) line-of-sight (LoS) blockage (iii) the effect of molecular absorption noise [4]–[6].

Large-scale antenna arrays and beamforming techniques have received a lot of attention in compensating for the propagation loss of THz signals and improving the coverage. One line of research in that area is gearing towards dealing with the beam squint effect caused by wide bandwidth in THz beamforming systems [7]–[9], under the assumption of plane wave propagation model, which applies to far-field scenarios where the distance between the transmitter and the receiver is greater than or equal to the Rayleigh distance of the antenna array, i.e., $2D^2/\lambda$ [10]. Here, D is the maximum dimension of the antenna array, and λ denotes the wavelength. However, this assumption may not hold true for most achievable THz communication or sensing distances. For instance, for an array size of $0.1m$, the Rayleigh distance is about $4m$ for an operating carrier frequency at 60 GHz. Meanwhile, this distance grows to approximately $20m$ at 0.3 THz. In that case, we refer to the scenario as the *near-field* one, where spherical wave propagation models should be taken into account.

Although spherical wavefronts have been extensively studied [10]–[12], the literature on *near-field* THz beamforming is relatively sparse [13], [14]. The work [13] follows the line of research in mmWave, and extends the joint two-level spatial multiplexing and beamforming scheme to THz communications for improving the spectral efficiency in pure LoS conditions. Different from lower frequencies, because of the quasi-optical traits of THz wave, the near field beams can focus them at a single focal point by a radially symmetric and linear-ramp field distribution [15]. The work [14] thus considers the beam focus problem for a THz circular planar array, and proposes a kind of frequency modulated waveform to mitigate the beam misfocus effect caused by wide bandwidth in THz beamforming systems.

To the best of the authors' knowledge, none of existing works discuss how the system parameters affect the beam focusing performance in the array near-field. Nevertheless, the spatial focus trait, if properly controlled, is useful in achieving physical-layer (PHY) security for proximal legitimate user and eavesdropper, and also is useful in reducing electromagnetic interference in networks. In this work, we consider a scenario in which a THz transmitter wishes to focus its beam to a desired spatial region. Our main contributions are summarized as follows.

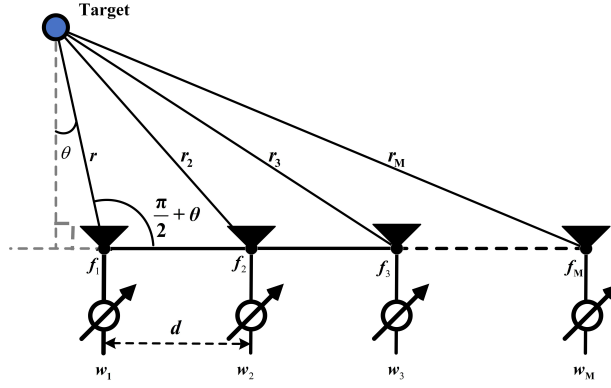


Fig. 1. Illustration of the frequency diverse array beamforming approach.

- 1) We obtain an analytically range-angle dependent beam focusing model for THz linear antenna arrays, uncovering that the achievable focusing spatial region constitutes a rotated ellipse centered at the target, with the x and y coordinates denoting the range and angle, respectively.
- 2) We determine the achievable coverage of the ellipse in closed form, as a function of the carrier frequency, the array dimension and the user's location, thus giving insight into how those system parameters affect the array's focusing performance.
- 3) It shows that due to ultra-short wavelength of THz waves, in the near-field the beam pattern transforms to an ellipse even with a conventional phased array. Further, we provide two distinct schemes for constructing carrier frequency offsets at antenna elements, through which we can control the beam focusing performance flexibly.

II. SYSTEM MODEL AND PROBLEM STATEMENT

As shown in Fig. 1, here we consider a THz transmitter that consists of an M -antenna uniform array, with the first antenna element at the origin, and a target user at the location (r, θ) . By applying cosine rule, the distance from the m -th antenna element to the target user is

$$\begin{aligned}
 r_m &= \sqrt{r^2 + (m-1)^2 d^2 + 2r(m-1)d \sin \theta} \\
 &\stackrel{(a)}{\approx} r + \frac{(m-1)^2 d^2}{2r} + (m-1)d \sin \theta.
 \end{aligned} \tag{1}$$

Here, the equation (a) holds true under the assumption of $(m-1)d \ll r$, that is, as compared with the distance r the array size is small enough.

The transmitter intends to forward information to the target user. As will be shown later in Fig. 2, when the carrier frequency f_c increases to THz, the angle dependent beam transforms to a range-angle dependent ellipse. Besides, noting that the frequency diverse beamforming scheme has been studied extensively in recent years for far-field radars [16]–[19], wherein results show that the frequency diverse array enables range-dependent radiation patterns. Therefore, in order to achieve flexible beam focusing in the range dimension, we consider the frequency diverse beamforming approach. Specifically, a carrier frequency offset Δf_m and a weight w_m are employed at the m th antenna element, respectively.

Let f_c be the carrier frequency, the radiation frequency of the m th antenna is thus $f_m = f_c + \Delta f_m$. In addition, the uniform antenna spacing of the transmit array is d , which is no less than half of the wavelength to avoid aliasing effects. The signal received at the target user can thus be expressed as

$$y(r, \theta; \mathbf{f}, \mathbf{w}) = \frac{1}{r} \sum_{m=1}^M w_m e^{j2\pi f_m r_m / c} \quad (2)$$

where the frequency offset vector $\mathbf{f} \triangleq [\Delta f_1, \Delta f_2, \dots, \Delta f_M]$ and $\mathbf{w} \triangleq [w_1, w_2, \dots, w_M]$.

The following assumptions are made in this paper.

- We assume that the difference in path-loss from antenna elements to the target user can be ignored, since although the difference in r_m s is comparable to the wavelength of THz, it is tiny in absolute value.
- We assume that as compared with the distance r the array size is small enough. This assumption is reasonable for most THz communication scenarios since the wavelength of THz is at the millimeter or even sub-millimeter level.
- We assume that independent frequency offsets can be applied to a large antenna array.

Same as in phased array, to maximize the antenna gain at the target user at (R_D, θ_D) , at the m th antenna we should set the weight $w_m^* = \exp(-j2\pi f_m r_m^D / c)$, where r_m^D is obtained by setting (r, θ) in (1) as (R_D, θ_D) . The resulting beampattern can thus be computed as,

$$S(r, \theta; \mathbf{f}) = \left| \sum_{m=1}^M e^{j2\pi f_m (r_m - r_m^D) / c} \right|^2. \quad (3)$$

Generally, the determination of the beampattern for near-field is a non-convex problem. For the purpose of exhibiting the results in a provable way, we introduce the half-power points,

i.e. the 3dB main lobe, as an alternative performance metric. That is, (R_B, θ_B) are those points where the received power reduces to half of that received by the target user, i.e.,

$$\mathcal{B} \triangleq \{(R_B, \theta_B) | S(R_B, \theta_B; \mathbf{f}) = M^2/2\}. \quad (4)$$

From (4), one can see that the achievable boundary of \mathcal{B} not only depends on the position of the target user, but also depends on the frequency offsets at the transmit antenna elements. In order to focus the transmitting energy on any desired spatial region, we need to find out how those factors affect the boundary of \mathcal{B} . In the following, we will first determine \mathcal{B} in closed form, and then giving two strategies to control the beampattern by adjusting the frequency offsets at transmit antenna elements.

III. THE RANGE-ANGLE DEPENDENT BEAM FOCUSING MODEL FOR THZ LINEAR ANTENNA ARRAY

In this section, we will derive the beampattern in closed-form, thus giving a beam focusing model and a way to analytically evaluate the beam focusing performance. The key idea is to reformulate the beampattern expression in (4) by employing theorem of analytic geometry (see *Lemma 1*), with which we show that the achievable spatial region constitutes a rotated ellipse centered at (R_D, θ_D) , with the x and y coordinates denoting R_B and θ_B , respectively. As such, the determination of the spatial region is reduced to a problem of deriving the coverage of a rotated ellipse. Then by *Theorem 1* we determine the achievable coverage of the rotated ellipse along the range dimension and angular dimension in closed form. Details are shown in the following text.

Lemma 1: For a THz linear array, the boundary of \mathcal{B} given in (4) satisfies the following equation:

$$\begin{aligned} X(R_B - R_D)^2 + 2Y(R_B - R_D)(\theta_B - \theta_D) + \\ Z(\theta_B - \theta_D)^2 - M^2 = 0, \end{aligned} \quad (5)$$

where X , Y and Z are given as follows.

$$\begin{aligned} X &= \frac{2\pi^2}{c^2} \sum_{m=1}^M \sum_{n=1}^M [2(\xi_m - \xi_n)]^2 \\ Y &= \frac{4\pi^2 df_c \cos \theta_D}{c^2} \sum_{m=1}^M \sum_{n=1}^M [2(\xi_m - \xi_n)(m - n)] \\ Z &= \frac{8\pi^2 f_c^2 d^2 \cos^2 \theta_D}{c^2} \sum_{m=1}^M \sum_{n=1}^M (m - n)^2, \end{aligned} \quad (6)$$

with $\xi_m = \Delta f_m - \frac{d^2 f_c}{2R_D^2}(m-1)^2, \forall m$.

Proof: See Appendix A. ■

Based on *Lemma 1*, one can see that the type of the half-power boundary is depended on the value of X , Y , and Z . From the geometry knowledge, it holds true that, if $XZ > Y^2$ the half-power boundary is an ellipse. Otherwise, the half-power boundary is a hyperbola or a pair of parallels for the case of $XZ < Y^2$ and $XZ = Y^2$, respectively. For the last two cases, it is impossible to achieve beam alignment in reality, which is of no interest to the communication community. Thus, in this paper we only focus on the first case where the half-power boundary is an ellipse.

Theorem 1: For a THz beam focusing system with linear antenna array, the achievable ellipse area, the main lobe beamwidth in the range and angle dimension are respectively,

$$S = \frac{\pi M^2}{\sqrt{XZ - Y^2}},$$

$$\Delta_R \triangleq \max(R_B) - \min(R_B) = 2\sqrt{\frac{M^2 Z}{XZ - Y^2}},$$

$$\Delta_\theta \triangleq \max(\theta_B) - \min(\theta_B) = 2\sqrt{\frac{M^2 X}{XZ - Y^2}}.$$

Proof: See Appendix B. ■

Specially, for the case without frequency offsets at antenna elements, i.e., $\Delta f_m = 0, \forall m$, we get a conventional phased array. Substituting $\Delta f_m = 0, \forall m$ into *Theorem 1*, we arrive at *Corollary 1* as follows.

Corollary 1: Provided that $\Delta f_m = 0, \forall m$, the frequency diverse array degenerates to a phased array, and the ellipse area, the main lobe beamwidth in the range and angle dimension are respectively,

$$S = \frac{3\sqrt{15}c^2 R_D^2}{\pi f_c^2 d^3 \cos \theta_D (M^2 - 1) \sqrt{M^2 - 4}}$$

$$\Delta_R = \frac{6\sqrt{10}c R_D^2}{\pi f_c d^2 \sqrt{(M^2 - 1)(M^2 - 4)}}$$

$$\Delta_\theta = \frac{c\sqrt{6}(16M^2 - 30M + 11)}{\pi f_c d \cos \theta_D \sqrt{(M^2 - 1)(M^2 - 4)}}$$

Remark 1: According to *Corollary 1*, one can see that the ellipse area of a phased array decreases as the number of antennas M increases, which indicates that as the carrier frequency f_c increases to THz, the angular dependent beam transforms to a range-angle dependent ellipse.

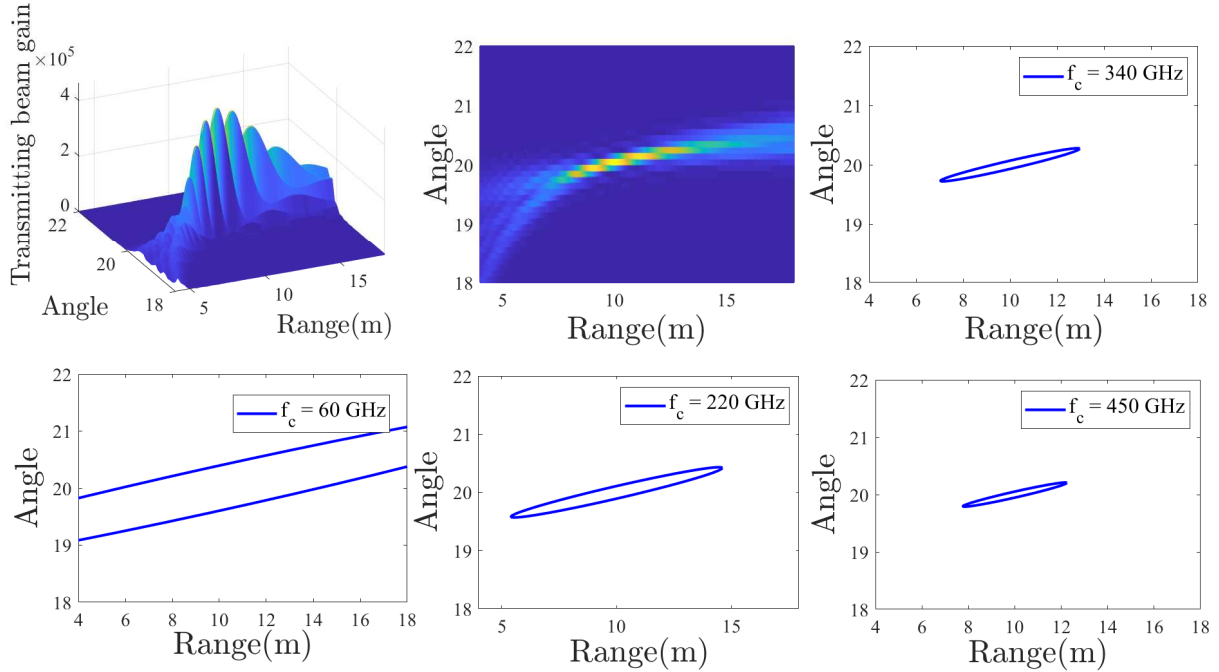


Fig. 2. Beam pattern of the phased array: transformation from beam to ellipse.

This coincides with the numerical results as shown in Fig. 2, where the array antenna size $D = 0.3m$, and a target user is at the location of $(R_D, \theta_D) = (10m, 20^\circ)$.

Remark 2: The main lobe beamwidth in the range dimension increases as the distance R_D from the transmitter increases, which indicates that as the target user moves from the near-field to the far-field range, the beam focusing ability declines. Furthermore, the main lobe beamwidth in the angular dimension is independent of the distance R_D .

Remark 3: The property of ultra-short wavelength of THz wave can be a double-edged sword. On the one hand, as compared to lower frequencies, THz phased array gets higher resolution and can focus RF signals to a two-dimensional spatial region instead of only along the angular direction. On the other hand, THz signals suffer from limited range coverage, which challenges the conventional beam scanning and tracking methods that only differentiate beams with respect to angular dimension.

IV. PROPOSED TRANSMISSION SCHEMES THAT CAN FOCUS BEAM FLEXIBLY

By *Theorem 1*, we show that the achievable spatial region constitutes an ellipse, with the x and y coordinates denoting R_B and θ_B , respectively. Furthermore, the achievable coverage of the

ellipse depends on system parameters such as the carrier frequency, the array dimension and the user's location. In this section, we give two distinct schemes for constructing carrier frequency offsets at antenna elements, through which the beam focusing performance is flexibly controlled.

As aforementioned, we only need to focus on the case where the half-power boundary is an ellipse and $XZ > Y^2$, which holds true if and only if

$$\Delta f_m \neq \frac{\beta m}{2} + \frac{f_c d^2}{2R_D^2}(m-1)^2 + C, \quad (7)$$

where β and C are constants. In other words, to make sure the energy is delivered to an intended two-dimensional spatial region, the only prerequisite is that the equation (7) holds true. Meanwhile, the specific value of Δf_m s decides the values of Δ_R and Δ_θ .

Proposition 1: Let $\Delta f_m = \frac{f_c d^2}{2R_D^2}\alpha(m-1)^2, \forall m$, then the main lobe beamwidth in the range and angle dimension are respectively

$$\Delta_R = \frac{2}{|1-\alpha|} \sqrt{\frac{M^2 Z_{pa}}{X_{pa} Z_{pa} - Y_{pa}^2}}$$

$$\Delta_\theta = 2 \sqrt{\frac{M^2 X_{pa}}{X_{pa} Z_{pa} - Y_{pa}^2}}$$

where α is an undermined parameter. X_{pa} , Y_{pa} and Z_{pa} equal X , Y and Z , respectively, by setting the frequency offsets in (6) as zero.

Proposition 2: Let $\Delta f_m = \frac{\delta}{2} \left| \frac{\sin(m-1)}{\pi} \right| + \frac{f_c d^2}{2R_D^2}(m-1)^2, \forall m$, then the main lobe beamwidth in the range and angle dimension are respectively

$$\Delta_R = \frac{2}{\delta} \sqrt{\frac{M^2 Z_{fa}}{X_{fa} Z_{fa} - Y_{fa}^2}}$$

$$\Delta_\theta = 2 \sqrt{\frac{M^2 X_{fa}}{X_{fa} Z_{fa} - Y_{fa}^2}}$$

where δ is an undermined parameter. X_{fa} , Y_{fa} and Z_{fa} equal X , Y and Z , respectively, by setting $\xi_m = \left| \frac{\sin(m-1)}{\pi} \right|$ in (6).

Substituting Δf_m into *Theorem 1* and by some mathematical reformulations, we get the conclusions as in *Proposition 1* and *Proposition 2*. This completes the proof.

It is obvious that for any intended range of $\Delta_R = \rho$, we can derive the specific value of α , δ , and frequency offsets by substituting $\Delta_R = \rho$ into *Proposition 1* and *Proposition 2*, respectively. The main lobe beamwidth in range dimension Δ_R decreases monotonically with $|1-\alpha|$ and δ , respectively. Meanwhile, the main lobe beamwidth in angular dimension Δ_θ remains a constant.

For example, let the carrier frequency be 340GHz, the array antenna size $D = 0.3m$, and a target user is at the location of $(R_D, \theta_D) = (15m, 20^\circ)$. By adjusting the parameters α and δ , we get different frequency offsets which are shown in Table 1 and Table 2, respectively. As a result, as shown in Fig. 3, the beam focusing performance is flexibly controlled.

TABLE I
PROPOSED SCHEME 1 WITH DIFFERENT α

α	$m = 1$	$m = 2$	$m = 3$	\dots	$m = 679$	$m = 680$
0.2	0	29.4Hz	117.6Hz	\dots	13.5MHz	13.6MHz
0.4	0	58.8Hz	235.3Hz	\dots	30.0MHz	27.1MHz
0.6	0	88.3Hz	352.9Hz	\dots	40.5MHz	40.7MHz
0.8	0	117.6Hz	470.6Hz	\dots	54.1MHz	54.2MHz

TABLE II
PROPOSED SCHEME 2 WITH DIFFERENT δ

δ	$m = 1$	$m = 2$	$m = 3$	\dots	$m = 679$	$m = 680$
6×10^7	0	8.0MHz	8.7MHz	\dots	72.9MHz	71.2MHz
12×10^7	0	16.1MHz	17.4MHz	\dots	78.1MHz	75.5MHz
18×10^7	0	24.1MHz	26.1MHz	\dots	83.4MHz	79.3MHz
24×10^7	0	32.1MHz	34.7MHz	\dots	88.7MHz	83.2MHz
30×10^7	0	40.1MHz	43.4MHz	\dots	93.9MHz	87.1MHz

Remark 4: It is worthwhile to note that there are many other feasible solutions to control the beam focusing performance. Due to the limited space, we only enumerate two of them and show that it is possible to flexibly focus the beam to a two-dimensional spatial region with a THz linear antenna array. In *Proposition 1* the frequency offsets over different antennas are integer times of a fundamental value, i.e., $f_c d^2 \alpha / 2R_D^2$. In comparison, *Proposition 2* needs more fine-grained frequency offsets over different antennas, which varies with the term $\sin(m-1)/\pi$, with m denoting the antenna index. On the other hand, current THz sources are produced with frequency multipliers, which only support coarse-grained frequency offsets. Therefore, from the

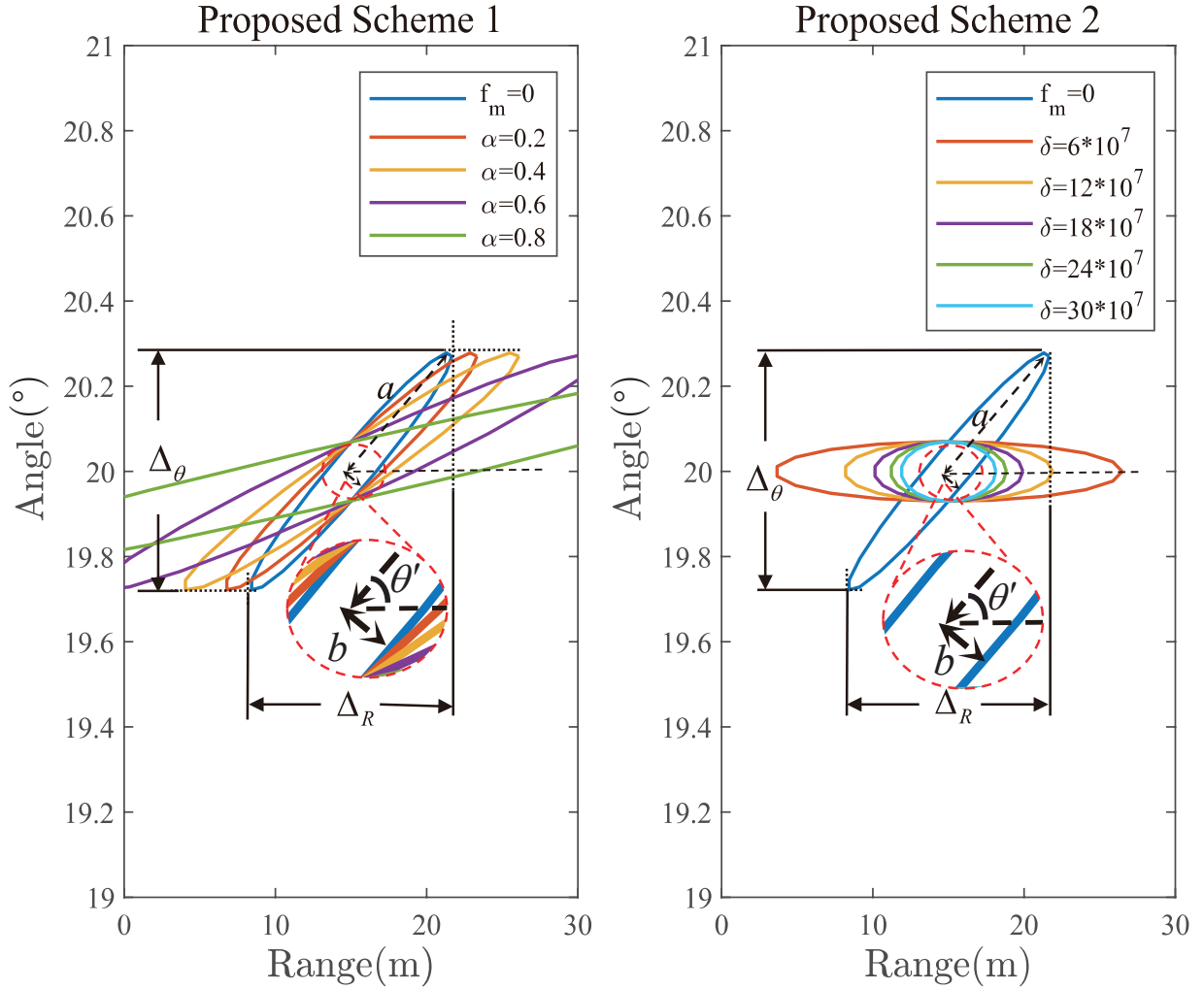


Fig. 3. Beampattern obtained with different parameters α or δ .

perspective of implementation, the realization of *Proposition 2* needs digital beamforming, which requires higher power consumption and higher system cost.

V. CONCLUSION

We have analytically addressed the beam focusing problem of a THz transmitter which wishes to focus its beam to a desired spatial region in the array near-field. Specifically, based on a theorem from analytic geometry, we have shown that the achievable spatial region constitutes an ellipse. We have further determined in closed form the achievable coverage of the ellipse, revealing how the system parameters such as the carrier frequency, the array dimension and the user's location affect its focusing performance. We have also given two schemes to analytically

control the coverage of the ellipse by adjusting carrier frequency offsets. Numerical results have validated the theoretical findings and demonstrate the performance of the proposed method.

APPENDIX A
PROOF OF *Lemma 1*

According to (4), the half-power boundary points of (R_B, θ_B) satisfies the following equation:

$$\begin{aligned}
\frac{M^2}{2} &= \left| \sum_{m=1}^M \exp \left(j \frac{2\pi f_m (r_m^B - r_m^D)}{c} \right) \right|^2, \\
&\stackrel{(a)}{=} \left(\sum_{m=1}^M e^{jx_m} \right) \left(\sum_{m=1}^M e^{jx_m} \right)^* \\
&\stackrel{(b)}{=} \sum_{n=1}^M \sum_{m=1}^M \cos(x_m - x_n), \\
&\stackrel{(c)}{\approx} \sum_{n=1}^M \sum_{m=1}^M \left(1 - \frac{1}{2}(x_m - x_n)^2 \right), \tag{8}
\end{aligned}$$

where (a) is obtained by letting $x_m = 2\pi f_m (r_m^B - r_m^D)/c$, with r_m^B obtained by setting (r, θ) in (1) as (R_B, θ_B) ; (b) holds true due to using Euler's Theorem; (c) is obtained by using the approximation $x_m \approx x_n$. This approximation is usually valid in THz near-field scenarios, where due to the quasi-optical traits of THz waves the half-power boundary points are assumed to be near the maximum power point. Therefore, the equation (8) can be re-expressed as

$$\sum_{m=1}^M \sum_{m=1}^M (x_m - x_n)^2 - M^2 = 0. \tag{9}$$

On the other hand, looking into the formula of $(x_m - x_n)^2$, we have the following derivations,

$$\begin{aligned}
(x_m - x_n)^2 &= \frac{4\pi^2}{c^2} \{ f_m (r_m^B - r_m^D) - f_n (r_n^B - r_n^D) \}^2 \\
&\stackrel{(a)}{=} \frac{4\pi^2}{c^2} \{ [f_c (r_m^B - r_m^D) + \Delta f_m (R_B - R_D)] \\
&\quad - [f_c (r_n^B - r_n^D) + \Delta f_n (R_B - R_D)] \}^2 \\
&\stackrel{(b)}{=} \frac{2\pi^2}{c^2} [2(\xi_m - \xi_n)]^2 (R_B - R_D)^2 \\
&\quad + \frac{2 \times 4\pi^2 d f_c \cos \theta_D}{c^2} [2(\xi_m - \xi_n)(m - n)] \\
&\quad (R_B - R_D)(\theta_B - \theta_D) \\
&\quad + \frac{8\pi^2 f_c^2 d^2 \cos^2 \theta_D}{c^2} (m - n)(\theta_B - \theta_D)^2, \tag{10}
\end{aligned}$$

where $\xi_m \triangleq \Delta f_m - \frac{d^2 f_c}{2R_D^2} (m - 1)^2, \forall m$. The equation (a) is obtained by substituting (1) into $(x_m - x_n)^2$, and applying the facts that $2\pi \Delta f_m (m - 1) d^2 / 2r$ and $2\pi \Delta f_m (m - 1) d \sin \theta$ are

small enough and can be omitted. The equation (b) is obtained by letting $(\sin \theta_B - \sin \theta_D) \approx \cos \theta_D (\theta_B - \theta_D)$, and executing the second-order Taylor expansion around (R_D, θ_D) , that is, (R_B, θ_B) . This can be done since the half-power boundary points are near the target user.

Substituting (10) into (9) and doing some reformulations, we arrive at conclusions in *Lemma 1*. This completes the proof.

APPENDIX B

PROOF OF *Theorem 1*

According to the theorem of analytic geometry [20], if an equation has the form given in (5), it must correspond to a rotated ellipse centered at (R_D, θ_D) , with the x and y coordinates denoting R_B and θ_B , respectively. Its area, semi-major and semi-minor axes are, respectively,

$$S = \pi ab = \pi M^2 / \sqrt{XZ - Y^2}, \quad (11a)$$

$$a = \sqrt{2M^2 / \left(X + Z - \sqrt{(X - Z)^2 + 4Y^2} \right)}, \quad (11b)$$

$$b = \sqrt{2M^2 / \left(X + Z + \sqrt{(X - Z)^2 + 4Y^2} \right)}. \quad (11c)$$

Moreover, the rotation angle of the ellipse from the x -axis, denoted by θ' , satisfies

$$\cos^2 \theta' = 1/2 + (Z - X)/2\sqrt{(X - Z)^2 + 4Y^2}.$$

The coordinates of the boundary point on the ellipse can thus be expressed as [21],

$$R_B = a \cos \theta' \cos t - b \sin \theta' \sin t + R_D, \quad (12a)$$

$$\theta_B = a \sin \theta' \cos t + b \cos \theta' \sin t + \theta_D, \quad (12b)$$

where $t \in [0, 2\pi]$.

Therefore, according to the auxiliary angle formula [22], the coverage of the ellipse in the range dimension and angle dimension are, respectively,

$$\begin{aligned} \Delta_R &= \max(R_B) - \min(R_B) = 2\sqrt{a^2 \cos^2 \theta' + b^2 \sin^2 \theta'} \\ &= 2\sqrt{M^2 Z / (XZ - Y^2)}, \end{aligned} \quad (13)$$

$$\begin{aligned} \Delta_\theta &= \max(\theta_B) - \min(\theta_B) = 2\sqrt{a^2 \sin^2 \theta' + b^2 \cos^2 \theta'} \\ &= 2\sqrt{M^2 X / (XZ - Y^2)}. \end{aligned} \quad (14)$$

Note that X , Y and Z are given by (6). This completes the proof.

REFERENCES

- [1] L. U. Khan, W. Saad, and et.al., “Digital-twin-enabled 6G: Vision, architectural trends, and future directions,” *IEEE Communications Magazine*, vol. 60, no. 1, pp. 74–80, Jan. 2022.
- [2] Z. Chen, C. Han, and et.al., “Terahertz wireless communications for 2030 and beyond: A cutting-edge frontier,” *IEEE Communications Magazine*, vol. 59, no. 11, pp. 66–72, Nov. 2021.
- [3] Y. Feng, B. Zhang, and et.al., “A 20.8-gbps dual-carrier wireless communication link in 220-ghz band,” *China Communications*, vol. 18, no. 5, pp. 210–220, May 2021.
- [4] C. Chaccour, M. S. Naderi, and et.al., “Seven defining features of terahertz (thz) wireless systems: A fellowship of communication and sensing,” *IEEE Communications Surveys & Tutorials*, pp. 1–1, Jan. 2022.
- [5] H. Sardeddeen, M.-S. Alouini, and T. Y.Al-Naffouri, “An overview of signal processing techniques for terahertz communications,” *Proceedings of the IEEE*, vol. 109, no. 10, pp. 1628–1665, Oct. 2021.
- [6] Z. Chen, X. Ma, and et.al., “A survey on terahertz communications,” *China Communications*, vol. 16, no. 2, pp. 1–35, Feb. 2019.
- [7] Q. Wan, J. Fang, Z. Chen, and H. Li, “Hybrid precoding and combining for millimeter wave/sub-THz MIMO-OFDM systems with beam squint effects,” *IEEE Transactions on Vehicular Technology*, vol. 70, no. 8, pp. 8314–8319, Aug. 2021.
- [8] J. Tan and L. Dai, “Wideband beam tracking in THz massive MIMO systems,” *IEEE Journal on Selected Areas in Communications*, vol. 39, no. 6, pp. 1693–1710, Jun. 2021.
- [9] A. M. Elbir, K. V. Mishra, and S. Chatzinotas, “Terahertz-band joint ultra-massive MIMO radar-communications: Model-based and model-free hybrid beamforming,” *IEEE Journal of Selected Topics in Signal Processing*, vol. 15, no. 6, pp. 1468–1483, Nov. 2021.
- [10] F. Bohagen, P. Orten, and G. E. Oien, “On spherical vs. plane wave modeling of line-of-sight MIMO channels,” *IEEE Transactions on Communications*, vol. 57, no. 3, pp. 841–849, Mar. 2009.
- [11] Z. Zhou, X. Gao, and et.al., “Spherical wave channel and analysis for large linear array in LoS conditions,” in *2015 IEEE Globecom Workshops (GC Wkshps)*, San Diego, CA, USA, Dec. 2015, pp. 1–6.
- [12] E. Björnson and L. Sanguinetti, “Power scaling laws and near-field behaviors of massive MIMO and intelligent reflecting surfaces.”
- [13] L. Yan, C. Han, and J. Yuan, “Joint two-level spatial multiplexing and beamforming in terahertz ultra-massive MIMO systems,” in *IEEE INFOCOM 2019-IEEE Conference on Computer Communications Workshops (INFOCOM WKSHPS)*, Paris, France, Apr. 2019, pp. 873–878.
- [14] N. J. Myers and R. W. Heath, “Infocus: A spatial coding technique to mitigate misfocus in near-field LoS beamforming,” *IEEE Transactions on Wireless Communications*, pp. 1–1, Sep. 2021.
- [15] D. Headland, Y. Monnai, and et.al., “Tutorial: Terahertz beamforming, from concepts to realizations,” *Apl Photonics*, vol. 3, no. 5, p. 051101, Nov. 2018.
- [16] W.-Q. Wang, “Frequency diverse array antenna: New opportunities,” *IEEE Antennas and Propagation Magazine*, vol. 57, no. 2, pp. 145–152, Apr. 2015.
- [17] Y. Ding, J. Zhang, and V. Fusco, “Frequency diverse array OFDM transmitter for secure wireless communication,” *Electronics Letters*, vol. 51, no. 17, pp. 1374–1376, Aug. 2015.
- [18] J. Lin, Q. Li, and et.al., “Physical-layer security for proximal legitimate user and eavesdropper: A frequency diverse array beamforming approach,” *IEEE Transactions on Information Forensics and Security*, vol. 13, no. 3, pp. 671–684, Mar. 2017.

- [19] Z. Ahmad, Z. Shi, and C. Zhou, "Time-variant focusing range-angle dependent beam pattern synthesis by uniform circular frequency diverse array radar," *IET Radar, Sonar & Navigation*, vol. 15, no. 1, pp. 62–74, Dec. 2021.
- [20] S. J. Leon, *Linear Algebra With Applications*. Pearson, 2015.
- [21] D. J. T and P. G, *Local analytic geometry: Basic theory and applications*. Springer Science & Business Media, 2013.
- [22] P. D. Barry, *Geometry with trigonometry*. Elsevier, 2001.